AJNR

Utility of Dual-Energy CT to Improve Diagnosis of CSF Leaks on CT Myelography following Lateral Decubitus Digital Subtraction Myelography with Negative Findings

S.J. Huls, D.P. Shlapak, D.K. Kim, S. Leng and C.M. Carr

AJNR Am J Neuroradiol published online 8 September 2022
http://www.ajnr.org/content/early/2022/09/08/ajnr.A7628

Published September 8, 2022 as 10.3174/ajnr.A7628

Utility of Dual-Energy CT to Improve Diagnosis of CSF Leaks on CT Myelography following Lateral Decubitus Digital Subtraction Myelography with Negative Findings

S.J. Huls, D.P. Shlapak, D.K. Kim, S. Leng, and C.M. Carr

ABSTRACT

SUMMARY: CSF leaks, including CSF-venous fistulas, which cause spontaneous intracranial hypotension, remain difficult to diagnose, even on digital subtraction myelography and CT myelography. Dual-energy CT technology has been used to improve diagnostic utility within multiple organ systems. The capability of dual-energy CT to create virtual monoenergetic images can be leveraged to increase conspicuity of contrast in CSF-venous fistulas and direct epidural CSF leakage to improve the diagnostic utility of CT myelography. Six cases (in 5 patients) are shown in which virtual monoenergetic images demonstrate a leak location that was either occult or poorly visible on high- or low-kilovolt series. This clinical report describes the novel application of dual-energy CT for the detection of subtle CSF leaks including CSF-venous fistulas.

ABBREVIATIONS: $CTDI_{vol}$ = volume CT dose index; CTM = CT myelography; CVF = CSF-venous fistula; DECT = dual-energy CT; DSM = digital subtraction myelography; LDDSM = lateral decubitus digital subtraction myelography; SIH = spontaneous intracranial hypotension; VMI = virtual monoenergetic images

Spontaneous intracranial hypotension (SIH) is caused by a CSF leak, commonly occurring in the thoracic spine.[1] CSF leaks can be classified into 4 types as shown by Farb et al:[2] ventral dural tears (type 1), proximal nerve root sleeve tears (type 2), CSF-venous fistulas (CVFs, type 3), and distal nerve root sleeve tears (type 4). A variety of techniques using prone or lateral digital subtraction myelography (DSM) and CT myelography (CTM) have been used to identify leaks, with institutions often preferring techniques that are familiar, developed locally, or based on access to equipment.[3] Despite improvements in the lateral decubitus digital subtraction myelography (LDDSM) technique, some patients with intracranial SIH findings on brain MR imaging do not have an identifiable leak on LDDSM or conventional CTM. Conventional CTM may show CVFs as hyperdense paraspinal veins or opacification of the vertebral venous plexus.[3-6] Even after thorough imaging investigation, some studies report a 50% detection rate, while others report detection rates as high as 87%.[2,7] In small or subtle CVFs, insufficient contrast resolution associated with a CSF leak compared with background remains a challenge.

Dual-energy CT (DECT) has numerous applications and is being increasingly used in multiple organ systems.[8] In neuroradiology, DECT has been shown to aid in differentiation of hemorrhage versus contrast, visualization of intracranial aneurysms, diagnosis of malignant sinonasal lesions, and metal artifact reduction.[9] In CTM, DECT has been studied as a mechanism to decrease metal artifacts and radiation exposure.[10] A major benefit of DECT is to reconstruct virtual monoenergetic images (VMI), which mimic images acquired with a monochromatic beam. VMI can be reconstructed at various kiloelectron volt energies (keV) that present different CT density values and image contrast due to the energy dependence of attenuation. For example, iodinated contrast has higher CT attenuation values, due to increased photoelectric effect, as keV levels approach the k-edge of iodine 33.2 keV.[11] Prior studies have demonstrated that 50–60 keV is the optimal energy level for higher attenuation of iodine-based contrast with minimally increased noise levels.[8] This is particularly beneficial for evaluation of CSF leaks in which contrast leakage is subtle. A recent case series by Houk et al[12] described the use of DECT for improved visualization of CSF leaks and CVFs. In this retrospective study, we present several additional cases illustrating the utility of DECT 50-keV VMI to diagnose CSF leaks on CTMs following negative findings on DSMs.

MATERIALS AND METHODS

Patient Selection

This was an institutional review board–approved, Health Insurance Portability and Accountability Act–compliant retrospective study. Informed consent was waived. From April 2019 to March 2021, diagnostic reports of LDDSMs with subsequent lateral decubitus CTMs performed at our institution were consecutively reviewed. Cases with questionable, possible, or equivocal CTM findings were

Received May 23, 2022; accepted after revision July 12.

From the Department of Radiology, Mayo Clinic, Ringgold Standard Institution, Rochester, Minnesota.

Please address correspondence to Sean Huls, MD, Mayo Clinic, 200 First St SW, Rochester, MN 55905; e-mail: huls.sean@mayo.edu

http://dx.doi.org/10.3174/ajnr.A7628

excluded. Cases in which LDDSM findings were negative and subsequent same-day CTM findings were positive were further reviewed, including imaging and patient history. The cases were reviewed separately by 3 board-certified neuroradiologists with 2, 4, and 8 years of experience and a first-year radiology resident; discordant findings were discussed; and a consensus decision was reached. Evaluation of each case was performed at the same window and level settings (W:1000 C:100; Visage Imaging). Cases in which DECT 50-keV VMI aided the diagnosis of subtle CSF leaks on CTM (after negative LDDSM findings) were included. At the site of extradural contrast, maximum and mean Hounsfield units were measured using an ROI of 5 mm for cases 1, 2, 3, and 4. A smaller ROI of 3 mm for case 5 to minimize overlap with osseous structures was used.

Imaging Technique

LDDSM was performed using the technique described by Kim et al.[13] Following the completion of each LDDSM with 11 mL of Omnipaque 300 (GE Healthcare), patients were immediately transferred to CT in the same decubitus position. A lateral decubitus CTM of the entire spine was performed with DECT. LDDSM and subsequent CTM were then repeated on the following day with the patient in the opposite lateral decubitus position, irrespective of whether a CVF was found on the first day. Our institution performs CTM on second- or third-generation dual-source DECT scanners (Somatom Definition Flash and Force; Siemens) (Table 1). CT acquisitions were performed with a 100/Sn 140-kV scanner (Somatom Definition Flash; Sn indicates a tin filter added to the high-kilovolt beam) or 100/Sn 150-kV scanner (Somatom Force). Routine axial, coronal, and sagittal bone and soft-tissue windows were reformatted, and 50-keV VMI were reconstructed with all source images reviewed in multi-planar reformat views.

RESULTS

Ten patients were identified with initial negative lateral decubitus DSM findings and subsequent positive CTM findings of CSF leak. Six examples in 5 patients were identified in which 50-keV VMI reformats were found to both qualitatively and quantitatively (increased Hounsfield units) improve the diagnosis of a CSF leak. Table 2 summarizes demographic data, symptoms, prior imaging findings, and treatment outcomes for each patient. Table 2 also contains CTM findings, including the presence of renal contrast in the renal collecting system, which is one of the features we use in our

Table 1: Parameters for CT cervical, thoracic, and lumbar spine myelogram (Siemens dual-source, dual-energy CT models)

DECT Model	Somatom Definition Flash	Somatom Force
Description	128-Section dual-source, dual-energy CT	192-Section dual-source, dual-energy CT
kV(p)	A: 100 B: Sn 140	A: 100 B: Sn 150
Quality reference mAs	A: 230 B: 178	A: 260 B: 130
Scan FOV (mm)	A: 500 B: 332	A: 500 B: 356
Rotation time (sec)	1.0	1.0
Pitch	0.9	0.9
Collimation (mm)	32 × 0.6	128 × .06

Table 2: Patient demographics, imaging findings, symptoms, treatment, and outcomes

Patient	Age	Sex	Other Imaging Findings	CTM Findings	Symptoms	Treatment	Outcome
1	28	F	High-probability brain MR imaging	T12-L1 CVF on left; T11-12 on right; contrast in the renal collecting system	Orthostatic headache, multifocal pain	T11 nerve root ligation	Initial relief with subsequent recurrence of symptoms in the setting of Marfan syndrome
2	50	M	Intermediate-probability brain MR imaging	CVF at left L2-3 and contrast in the renal collecting system	Orthostatic headache	Blood patch, transvenous embolization of the left L2 paraspinal vein	Dramatic symptom improvement following embolization
3	52	M	High-probability brain MR imaging, positive cisternogram findings	Right T10 distal nerve root sleeve tear with extradural contrast first detected at L2-3	Orthostatic headache, vision changes, pulsatile tinnitus	Hemi-laminectomy right T10-11, repair of CSF leak	Complete symptom resolution sustained for at least 1 year
4	34	F	Intermediate-probability brain MR imaging	Focus of CSF leak arising from the right lateral thecal sac at T7-8 thought to represent dural tear; contrast in the renal collecting system	Orthostatic headache, facial and hand paresthesia	Three targeted blood patches	Improvement after 3 targeted blood patches with recurrence of symptoms
5	50	F	Multiple nerve root diverticula on spine MR imaging	Faint linear hyperattenuation extending from a right T11-12 nerve sleeve diverticulum thought to represent CVF	Orthostatic headache, vision changes	Two targeted and 1 multifocal blood patch	Transient improvement after 2 targeted and 1 multifocal blood patch

Note:—M indicates male; F, female.

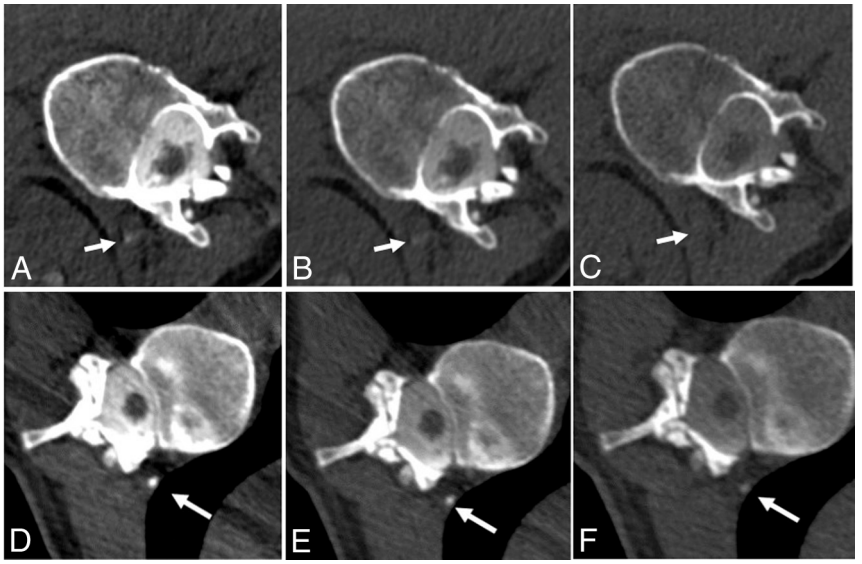

FIG 1. *A*, 50-keV VMI. *B*, 100 kV. *C*, 140 kV. Case 1: Left-side-down CTM with linear contrast at the left T12–L1 neural foramen, thought to reflect a CVF (*arrows*). Contrast is also noted in the renal collecting system. ROI Hounsfield units: *A*, 50-keV VMI Hounsfield unit maximum (max): 283 HU; mean, 76 HU. *B*, 100 -kV Hounsfield unit max: 147 HU; mean, 68 HU. *C*, 140-kV Hounsfield unit max: 116 HU; mean, 46 HU. *D*, 50-keV VMI. *E*, 100 kV. *F*, 140 kV. Case 1: Right-side-down CTM with paraspinal contrast at the level of T11–12, representing a second CVF (*arrows*). ROI Hounsfield units: *D*, 50-keV VMI Hounsfield unit max: 981 HU; mean, 693 HU. *E*, 100-kV Hounsfield unit max: 542 HU; mean, 369 HU. *F*, 140-kV Hounsfield unit max: 233 HU; mean, 107 HU.

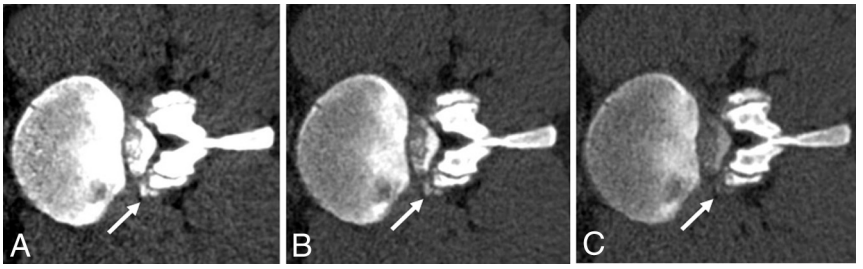

FIG 2. *A*, 50-keV VMI. *B*, 100 kV. *C*, 140 kV. Case 2: Left-side-down CTM with a suspected distal nerve root sleeve tear at the left L2–3 (*arrows*). The patient also had contrast in the renal collecting system (not shown). ROI Hounsfield units: *A*, 50-keV VMI Hounsfield unit maximum (max): 806 HU; mean, 271 HU. *B*, 100-kV Hounsfield unit max: 435 HU; mean, 133 HU. *C*, 140-kV Hounsfield unit max: 210 HU; mean, 68 HU.

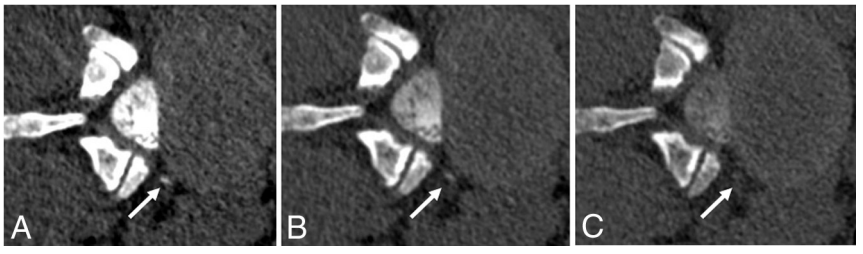

FIG 3. *A*, 50 -keV VMI. *B*, 100 kV. *C*, 150 kV. Case 3: Right-side-down CTM with linear contrast at the right L2–3 neuroforamen (*arrows*), extending into the paraspinal soft tissues, thought to reflect a vessel associated with contrast leakage at a higher right-T10 distal nerve root sleeve tear (not shown). ROI Hounsfield units: *A*, 50-keV VMI Hounsfield unit maximum (max): 485 HU; mean, 118 HU. *B*, 100-kV Hounsfield unit max: 271 HU; mean, 51 HU. *C*, 150-kV Hounsfield unit max: 151 HU; mean, 16 HU.

practice to increase our confidence in subtle or equivocal findings. These cases are illustrated in Figs 1–5, with 140-/150-kV, 100 -kV, and 50-keV VMI. Maximum and mean CT attenuation values (Hounsfield units) over the CSF leak ROIs are reported in the figure legends and Table 3 for each kilovolt peak level and 50-keV VMI reconstructions. For the 5 patients included in this study, the mean volume CT dose index ($CTDI_{vol}$) was 14.5 mGy (range, 13.2–15.6 mGy), the mean dose-length product was 1047.8 mGy × cm (range, 950.6–1150.5 mGy × cm), and the corresponding effective dose (using a K factor of 0.015 mSv/mGy × cm) was 15.7 mSv (range, 14.3–17.3 mSv).

Case 1

A 28-year-old woman with a history of Marfan syndrome developed symptoms of orthostatic headache and multifocal pain 6 years before presentation. MR imaging of the brain showed effacement of the suprasellar and prepontine cisterns, decreased mamillopontine distance, and diffuse dural enhancement and thickening, all indicating SIH (high-probability Bern Score = 6). A high-probability score is a Bern score of >5, based on MR imaging findings of SIH as described in Dobrocky et al.[14] She subsequently underwent LDDSM followed by CTM, which showed a left T12-L1 hyperdense paraspinal vein. Next-day right-side-down LDDSM followed by CTM showed a right hyperdense paraspinal vein at T11-12. Preoperative-planning CTA identified the artery of Adamkiewicz on the left at T12-L1, which prevents nerve root ligation. She underwent packing with venous obliteration of the veins on the left at T12-L1 and nerve root ligation on the right at T11-12. She had transient improvement, but due to her Marfan syndrome, she developed recurrent symptoms and intracranial stigmata of SIH indicating a new leak.

Case 2

A 50-year-old man had a 6-year history of consistently orthostatic symptoms of which headaches were the predominant symptom. At an outside institution, he was initially thought to have a Chiari I deformity related to his low-lying

FIG 4. *A*, 50-keV VMI. *B*, 100 kV. *C*, 140 kV. Case 4: Right-side-down CTM with a small focus of extradural contrast at the right aspect of the thecal sac at T7–8 (*arrows*). ROI Hounsfield units: *A*, 50-keV VMI Hounsfield unit maximum (max): 441 HU; mean, 275 HU). *B*, 100-kV Hounsfield unit max: 277 HU; mean, 165 HU. *C*, 140-kV Hounsfield unit max: 163 HU; mean, 102 HU.

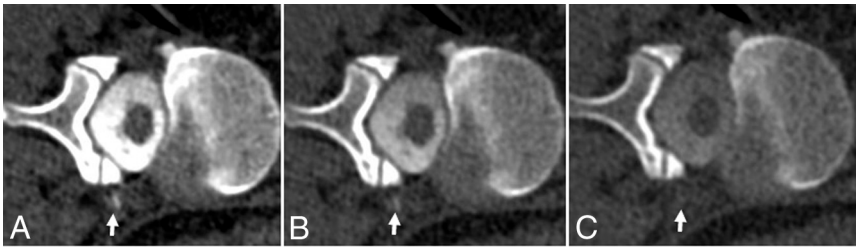

FIG 5. *A*, 50-keV VMI. *B*, 100 kV. *C*, 140 kV. Case 5: CTM right-side-down at the level of T11–12 shows linear focus most consistent with a CSF venous fistula (*arrows*). ROI Hounsfield units: *A*, 50-keV Hounsfield unit maximum (max): 436 HU; mean, 154 HU. *B*, 100-kV Hounsfield unit max: 251 HU; mean, 88 HU. *C*, 140-kV Hounsfield unit max: 125 HU; mean, 33 HU.

cerebellar tonsils, leading to a posterior fossa decompression, C2 laminectomy, and C3-4 laminoplasties 1 year before presentation. Nuclear medicine indium-111 (^{111}In) dethylenetriaminepentaacetic acid cisternogram obtained at our institution was positive for the presence of a CSF leak. MR imaging of the brain showed effacement of the suprasellar and prepontine cisterns and decreased mamillopontine distance (intermediate-probability Bern Score = 4).[14] His left lateral decubitus CTM following negative findings on LDDSM showed irregular contrast within the left L2-3 neural foramen. The patient underwent 2 targeted blood patches resulting in 2–4 weeks of symptom improvement. This was followed by transvenous Onyx (Medtronic) embolization with near-complete resolution of symptoms.

Case 3

A 52-year-old man had a 5-month history of orthostatic headache and pulsatile tinnitus after having his back "cracked" (physical manipulation) at home. He underwent 2 blood patches for presumed CSF leak with transient 2 weeks of partial symptomatic improvement. MR imaging of the brain showed pachymeningeal enhancement, venous sinus engorgement, and effacement of the suprasellar and prepontine cisterns (high-probability Bern score = 7).[14] An ^{111}In-DTPA cisternogram showed delayed radionuclide activity ascent supporting SIH. Right LDDSM had negative findings while subsequent same-side-down CTM showed subtle contrast extravasation along the right at L2–3. Subsequent dedicated lateral decubitus dynamic CTM, for localization, demonstrated that the leak originated at T10. A hemilaminectomy and right T10–11 nerve root ligation resulted in durable and sustained complete symptom relief for more than a year.

Case 4

A 34-year-old woman had postural orthostatic tachycardia syndrome and a 1-year history orthostatic headache and facial and hand paresthesias. Opening pressure with the patient in the prone position was low, measuring 8 cm of water (normal range, 10–25cm);[15] however, opening pressure is variable and not necessarily low in patients with definite CSF leaks. Head MR imaging demonstrated effacement of the suprasellar and prepontine cisterns (intermediate-probability Bern score = 3).[14] Initial right-side-down LDDSM had negative findings, but subsequent CTM showed subtle extradural contrast along the right aspect of the T7–8 neural foramen. Targeted CT-guided epidural blood patches resulted in dramatic reduction in headaches for approximately 8 months. Follow-up CTM after LDDSM again showed extradural contrast on the right at T7–8. The patient underwent Onyx embolization and had improved near-resolution of symptoms, compared with the blood patch.

Case 5

A 50-year-old woman had a 2-year history of orthostatic headache. She had 2 prior targeted blood patches. No recent brain MR imaging was available. Full-spine MR imaging showed multiple nerve root diverticula. CTM after negative DSM findings showed multiple nerve root diverticula with faint linear hyperdensity extending from a right T11–12 nerve sleeve diverticulum, suspicious for a CVF. She underwent a T11–12 targeted blood patch without changes in symptoms.

DISCUSSION

DECT has been commercially available with various technical implementations by different vendors.[16] With measurements from 2 different spectra, DECT enables material characterization and quantification, which has been used in many clinical areas, such as detection of gout, differentiation of renal stones, bone and plaque removal, iodine maps, and virtual noncontrast images.[16] Another major application of DECT is to generate VMI, which mimic the appearance of those images acquired with a monoenergetic beam. VMI at different energies (keV) have different image contrast, with lower kiloelectron volt VMI having higher iodine contrast due to increased photoelectric effect near the K-edge of iodine. These low-kiloelectron volt VMI (eg, 50 keV) have been found to be beneficial to improve image quality, decrease necessary iodinated contrast volume, and reduce the radiation dose. In this study, we aimed for a special application using low-kiloelectron volt VMI for improved detection of subtle differences in attenuation. As evidenced by the findings, 50-keV VMI have the highest CT attenuation value, followed by 100-kV single-energy images, and the lowest CT attenuation value at 140–150 kV.

Table 3: Hounsfield measurements at the site of contrast leak or CVF

Case	50 keV VMI Mean	50 keV VMI Max	100 kV Mean	100 kV Max	140/150 kV Mean	140/150 kV Max
Case 1L	76	283	68	147	46	116
Case 1R	693	981	369	542	107	233
Case 2	271	806	133	435	68	210
Case 3	118	485	51	271	16	150
Case 4	275	441	165	277	102	163
Case 5	154	436	88	251	33	125

Note:—1L indicates left side down CTM; 1R, right side down CTM

A potential downside of DECT, compared with single-energy CT, is an increased ionizing radiation dose. There is a paucity of literature comparing single-energy CTM with dual-energy CTM; however, one study comparing radiation exposures showed dual-energy CTM to have 1.6–1.9 times higher dose-length product and $CTDI_{vol}$ levels in comparison with single-energy CT in the cervical and thoracic spine. In the same study, whole-spine CTM performed with a strictly single-energy CT–capable scanner (Somatom Definition AS+; Siemens) showed a whole-spine mean $CTDI_{vol}$ of 13.99 mGy (range, 10.13–16.15 mGy) and a dose-length product of 837.8 (range, 530.5–1033.0).[17] As expected, these data suggest that DECT results in modest-to-moderate increased radiation exposure.

It is increasingly recognized that there is a subset of patients with intermediate or high-probability Bern scores on head MR imaging and a clinical diagnosis of SIH in whom a radiographically visible leak cannot be found despite multiple myelographic techniques. Given this difficulty of diagnosing apparently radiographically occult CSF leaks, any technique that can improve the diagnostic yield and visualization of subtle findings is critical. The provided examples in this case series demonstrate subtle areas of extradural contrast on CTM that are either best seen or only seen on the 50-keV VMI. DECT improves diagnostic accuracy by increasing the conspicuity of extradural contrast against the background. Correlating the appearance of a suspected CSF leak at different energy levels allows delineation of extradural iodine from other hyperattenuating structures such as osteophytes, heterotopic calcifications, and artifactual volume averaging. Our results are concordant with those of a recent smaller case series by Houk et al[12] showing improved visualization of subtle CSF leaks on CTM using VMI reformats.

CONCLUSIONS

This retrospective series is limited by the small number of cases. However, it adds to the existing literature showing that this novel use of DECT can aid in the radiographic evaluation of SIH. Given the intrinsic challenges of finding subtle CSF leaks, neuroradiologists need to have many tools in their arsenal. This case series would support further investigation for the applications of DECT in the setting of SIH. In addition, if available, routine use of dual-energy technology with virtual monoenergetic images reconstructed at 50 keV for detection of subtle CSF leaks has the potential of diagnosing a leak that would otherwise be missed with conventional imaging.

Disclosure forms provided by the authors are available with the full text and PDF of this article at www.ajnr.org

REFERENCES

1. Schievink WI, Meyer FB, Atkinson JL, et al. **Spontaneous spinal cerebrospinal fluid leaks and intracranial hypotension.** *J Neurosurg* 1996;84:598–605 CrossRef Medline
2. Farb RI, Nicholson PJ, Peng PW, et al. **Spontaneous intracranial hypotension: a systematic imaging approach for CSF leak localization and management based on MRI and digital subtraction myelography.** *AJNR Am J Neuroradiol* 2019;40:745–53 CrossRef Medline
3. Mamlouk MD, Ochi RP, Jun P, et al. **Decubitus CT myelography for CSF-venous fistulas: a procedural approach.** *AJNR Am J Neuroradiol* 2021;42:32–36 CrossRef Medline
4. Kim DK, Carr CM, Benson JC, et al. **Diagnostic yield of lateral decubitus digital subtraction myelogram stratified by brain MRI findings.** *Neurology* 2021;96:e1312–18 CrossRef Medline
5. Kranz PG, Gray L, Malinzak MD, et al. **CSF-venous fistulas: anatomy and diagnostic imaging.** *AJR Am J Roentgenol* 2021;217:1418–29 CrossRef Medline
6. Clark MS, Diehn FE, Verdoorn JT, et al. **Prevalence of hyperdense paraspinal vein sign in patients with spontaneous intracranial hypotension without dural CSF leak on standard CT myelography.** *Diagn Interv Radiol* 2018;24:54–59 CrossRef Medline
7. Kranz PG, Luetmer PH, Diehn FE, et al. **Myelographic techniques for the detection of spinal CSF leaks in spontaneous intracranial hypotension.** *AJR Am J Roentgenol* 2016;206:8–19 CrossRef Medline
8. Albrecht MH, Vogl TJ, Martin SS, et al. **Review of clinical applications for virtual monoenergetic dual-energy CT.** *Radiology* 2019;293:260–71 CrossRef Medline
9. Postma AA, Das M, Stadler AA, et al. **Dual-energy CT: what the neuroradiologist should know.** *Curr Radiol Rep* 2015;3:16 CrossRef Medline
10. Grams AE, Sender J, Moritz R, et al. **Dual energy CT myelography after lumbar osteosynthesis.** *Rofo* 2014;186:670–74 CrossRef Medline
11. De Cecco CN, Boll DT, Bolus DN, et al. **White paper of the Society of Computed Body Tomography and Magnetic Resonance on dual-energy CT, Part 4: abdominal and pelvic applications.** *J Comput Assist Tomogr* 2017;41:8–14 CrossRef Medline
12. Houk JL, Marin DM, Malinzak MD, et al. **Dual energy CT for the identification of CSF-venous fistulas and CSF leaks in spontaneous intracranial hypotension: report of four cases.** *Radiol Case Rep* 2022;17:1824–29 CrossRef Medline
13. Kim DK, Brinjikji W, Morris PP, et al. **Lateral decubitus digital subtraction myelography: tips, tricks, and pitfalls.** *AJNR Am J Neuroradiol* 2020;41:21–28 CrossRef Medline
14. Dobrocky T, Grunder L, Breiding PS, et al. **Assessing spinal cerebrospinal fluid leaks in spontaneous intracranial hypotension with a scoring system based on brain magnetic resonance imaging findings.** *JAMA Neurol* 2019;76:580–87 CrossRef Medline
15. Whiteley W, Al-Shahi R, Warlow CP, et al. **CSF opening pressure: reference interval and the effect of body mass index.** *Neurology* 2006;67:1690–91 CrossRef Medline
16. McCollough CH, Leng S, Yu L, et al. **Dual- and multi-energy CT: principles, technical approaches, and clinical applications.** *Radiology* 2015;276:637–53 CrossRef Medline
17. Zensen S, Bos D, Opitz M, et al. **Single- and dual-source CT myelography: comparison of radiation exposure and establishment of diagnostic reference levels.** *Diagnostics (Basel)* 2021;11:1809 CrossRef Medline